

Article

Study on Continuously Weakening Mechanism of Heap Leaching Velocity of Weathered Rare Earth Ores with the Increase of Ore Burial Depth

Defeng Liu ^{1,2}, Wenxin Yan ¹, Zhenyue Zhang ^{1,2,*}, Wenda Guo ^{1,2} and Ruan Chi ^{1,2}¹ School of Resource and Safety Engineering, Wuhan Institute of Technology, Wuhan 430073, China² Key Laboratory for Green Chemical Process of Ministry of Education, Wuhan Institute of Technology, Wuhan 430073, China

* Correspondence: zyzxmu@wit.edu.cn

Abstract: The column leaching experiments, CT, numerical simulation and fractal theory were adopted to study the continuously weakening mechanism of the heap leaching velocity of weathered rare earth ores with the increase of ore burial depth. The variation characteristics of pore structure and the seepage law of solution in ore samples at different depths during leaching were explored, respectively. The results showed that the variation of characteristic parameters of the pore structure in the lower ore samples was the main reason for the decrease in the leaching velocity. For the lower ore samples after leaching, the number of pores with a pore volume of less than 0.01 mm³ and a pore radius of less than 0.8 mm increased, while pore connectivity, the fractal dimension of the pore shape, the ratio of pore length to width and pore throat length reduced. The solution paths of the upper and middle ore samples were concentrated while that of the lower samples were few, even interrupted. The pore pressure of the ore samples decreased after leaching, especially that of the lower ore samples. The research results are helpful to enrich the basic theory on the heap leaching of weathered rare earth ores.

Keywords: weathered rare earth ores; leaching velocity; pore structure; micro-CT

Citation: Liu, D.; Yan, W.; Zhang, Z.; Guo, W.; Chi, R. Study on Continuously Weakening Mechanism of Heap Leaching Velocity of Weathered Rare Earth Ores with the Increase of Ore Burial Depth. *Minerals* **2023**, *13*, 581. <https://doi.org/10.3390/min13040581>

Academic Editor: Luis A. Cisternas

Received: 26 March 2023

Revised: 15 April 2023

Accepted: 17 April 2023

Published: 21 April 2023



Copyright: © 2023 by the authors. Licensee MDPI, Basel, Switzerland. This article is an open access article distributed under the terms and conditions of the Creative Commons Attribution (CC BY) license (<https://creativecommons.org/licenses/by/4.0/>).

1. Introduction

Rare earth elements are extremely valuable strategic resources, which are widely used in aerospace, military industry, new permanent magnetic materials and other fields, especially the medium and heavy rare earth elements occurring in weathered crust elution-deposited rare earth ores, generally shortened to weathered rare earth ores [1]. As this type of rare earth element is mainly adsorbed on the surface of clay minerals by hydrated or hydroxyl hydrated ions, it is impossible to recover medium and heavy rare earth resources through conventional beneficiation methods. At present, rare-earth ions are usually extracted through the ion exchange method [2]. Since weathered rare earth ore was found in the Zudong area, Longnan County, Ganzhou City, Jiangxi Province, China in 1969, leaching technology has expanded with the development of barrel leaching, pool leaching, heap leaching and in situ leaching. Nowadays, only heap leaching and in situ leaching technologies are applied in the field [3]. The in situ leaching technology has the characteristics of a low labor intensity, low production cost and fast ecological environment recovery, which has been widely promoted and applied. However, heap leaching technology is still required to recover the rare earth elements for the weathered rare earth ores without stable rock floors [4]. In the heap leaching process, the leaching velocity of the ores was slow because of a large number of fine particles and the poor permeability of the ores, which not only lengthened the leaching cycle and increased the leaching agent solution, but also seriously affected the leaching efficiency of the rare earth ores [5,6].

Given the above problems, scholars have conducted much research on the factors affecting the leaching velocity of rare earth ores. Column leaching experiments were performed by He et al. [7] to study the effects of concentration, pH and temperature on the seepage law of solution. It was found that the smaller the concentration and the higher the temperature, the better the permeability of the ore samples. The optimal leaching parameters were as follows: the concentration of ammonium ion was 0.2 mol/L, the pH was 4~8, the temperature was 25 °C and the injection velocity was 0.5 mL/min. To improve the seepage velocity of the solution and reduce the ammonia nitrogen pollution, Xiao et al. [8] and Chen et al. [9] developed the leaching agent of magnesium salt. In addition, Zhang et al. [10] studied the influence of carboxylate on the permeability and expansion characteristics of rare ores. They found that carboxylate not only showed high permeability but also had an anti-expansion effect. It was helpful to shorten the recovery cycle of the rare earth ores. In addition to the chemical factors, such as the leaching agent which affected the leaching velocity of the solution in the process of heap leaching, physical factors, such as particle gradation, also influenced it. The permeability characteristics of weathered rare earth ore samples with different particle sizes were studied by Luo et al. [11], who found that the decrease in the permeability coefficient of rare ores after leaching was due to particle migration blocking the pore throat. They suggested that the percolation behaviors of the solution could be regulated by controlling the particle migration. Wang et al. [12] believed that ion exchange and solution seepage caused the adsorption–desorption behavior of the microparticles, resulting in changes in the pore structure. It affected the permeability coefficient of rare earth ores, which could be controlled by adjusting the ion concentration. Deng et al. [13] studied the effect of the microparticle migration of rare earth ores on the permeability coefficient. It was found that controlling the injection strength could improve the leaching velocity of the rare earth ores.

The above research results provided a theoretical reference for improving the leaching velocity of the heap leaching of weathered rare earth ores. In addition, under the conditions of chemical factors, such as the best pH, and physical factors, such as the optimal injection strength, the leaching velocity of rare earth ores at different depths also gradually decreased and tended to be stable with the increase of the leaching time [14]. However, no scholars have explored why the above phenomenon occurred. Therefore, it was of great scientific significance and engineering practice value to study the continuously weakening mechanism of the heap leaching velocity of the weathered rare earth ores with the increase of ore burial depth.

Revealing the solution seepage mechanism from a microscopic perspective generally requires the use of advanced instruments and equipment, such as micro computed tomography (micro-CT), etc. It utilizes the X-ray absorption differences of materials with different densities to achieve a three-dimensional reconstruction of experimental samples. It was not only used in the fields of mining engineering and geotechnical engineering [15,16], but also in solution mining. Yin et al. [17] studied the two-dimensional and three-dimensional pore structure parameters of undisturbed rare earth ores by using micro-CT. It was found that the number of small pores accounted for a large proportion and determined the seepage law of the solution. In addition, researchers have found that combining CT and AVIZO software could effectively describe the pore structure and solution percolation paths from a microscopic perspective [18,19]. It effectively combined the reconstruction function of CT with the visualization advantages of AVIZO. In addition, it can also achieve quantitative analysis.

As a result, four kinds of reconstituted weathered rare earth ores were taken as the research objects in this paper. Through the column leaching experiments, CT, numerical simulation and fractal theory, the variation law of the characteristic parameters of the pore structure of ore samples at different depths during leaching were analyzed from a microscopic perspective. In addition, the variation characteristics of both the solution seepage path and pore pressure were explored. The research results could provide theoretical

support for improving the leaching velocity of the weathered rare earth ores in the heap leaching process.

2. Experimental

2.1. Raw Ore Characteristics

The raw ore was selected from a weathered rare earth ore in Fujian Province, China. The distribution characteristics of the particle gradation and corresponding characteristic parameters of the raw ore were obtained through a Winner 2308 automatic laser particle sizer, as shown in Figure 1. It showed that the particle size distribution was very uniform. The ore particle size was mainly small, and content below 2.00 mm accounted for 70%. The curvature coefficient was 1.11, and the non-uniformity coefficient was 20.89. This indicated that the grain size grading of the raw ore was good [20]. In addition, the rare earth ores' specific gravity (G_s) was measured as 1.16 g/cm^3 . Its moisture content (W_w) was 12.37%.

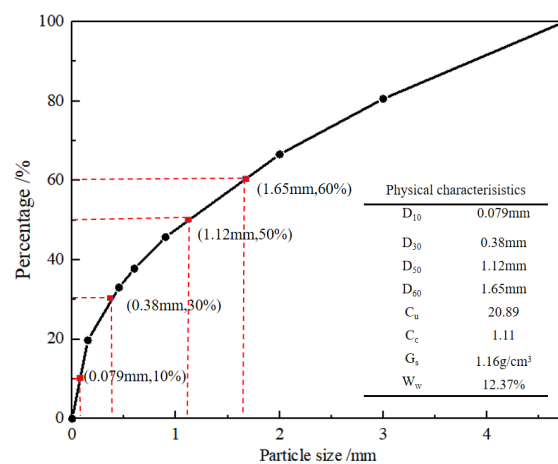


Figure 1. The size distribution of weathered rare earth ores, including its key physical characteristics.

Additionally, the main mineral composition and content of the raw ore were obtained using XRD (X-ray diffraction). It was seen that the main composition was quartz, kaolinite and illite, the content of which accounted for 52.8%, 28.5% and 18.7%, respectively, as shown in Figure 2.

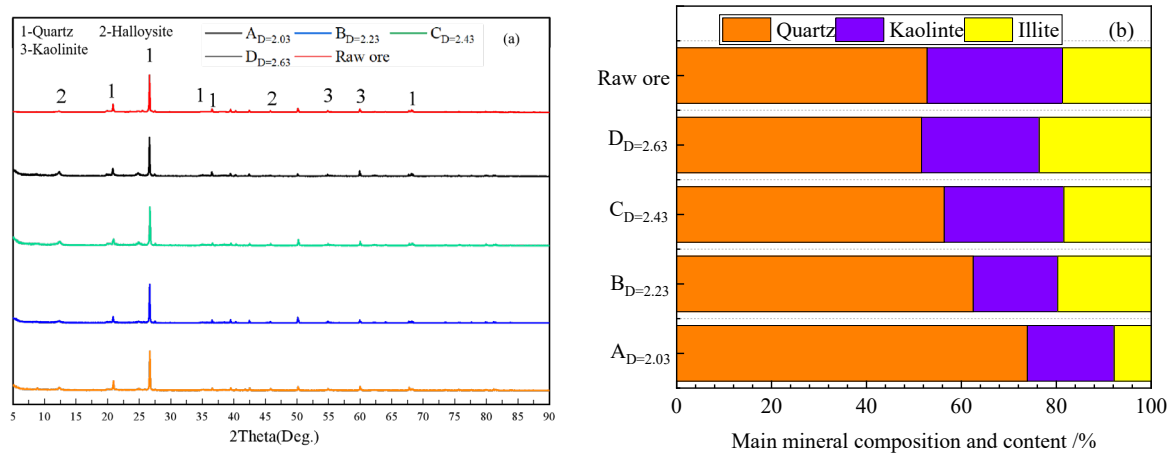


Figure 2. Main mineral composition and content of ore samples. (a) XRD profiles of ore samples; (b) Mineral content.

2.2. Experimental Samples

Fractal characteristics could be used to describe the complex and similar geometric structure, meaning that each component was a reduced overall shape. Liu et al. [21] found that the particle size distribution of the weathered crust elution-deposited rare earth ore had fractal characteristics. It can be quantitatively described by the fractal dimension obtained from Equation (1):

$$\frac{M(r < R_i)}{M_T} = \left(\frac{R_i}{R_{max}}\right)^{3-D} \tag{1}$$

where $M(r < R_i)$ represented the mass of the samples with a particle size of less than R_i , M_T represented the total mass of the samples, R_{max} was the maximum particle size of the samples and D represented the fractal dimension.

To study the weakening mechanism of the leaching velocity of the weathered rare earth ore, four kinds of samples with different size distribution characteristics were prepared based on fractal theory. Firstly, the raw ore was screened through a standard sieve according to the particle sizes of -0.15 mm, $+0.15\sim-0.90$ mm, $+0.90\sim-2.00$ mm and $+2.00$ mm, respectively, as shown in Figure 3. Secondly, the screened ores were recombined into 120 g ore samples with fractal dimensions of 2.03, 2.23, 2.43 and 2.63, which were named A, B, C and D, respectively, as shown in Figure 3. Their main mineral composition and content are shown in Figure 2. In addition, the mass percentage of four kinds of reconstituted ore samples within each particle size range was shown in Figure 4. Where the red represented a -0.15 mm particle size, the blue represented a $+0.15$ mm ~-0.90 mm particle size, the green represented a $+0.90$ mm ~-2.00 mm particle size and the black represented $+0.20$ mm particle size.

Figure 4 showed that the size distribution characteristics of the reconstituted ore samples were different, which could represent the weathered crust elution-deposited rare earth ores at four different locations. The sequence of four kinds of ore samples was $A < B < C < D$, according to the content of the fine particles (-0.15 mm). In addition, it was known from Figure 4 that the content of fine particles increased with the increase of the fractal dimension of particle gradation [21]. For example, the content of fine particles (-0.15 mm) in ore sample D with the largest fractal dimension reached 27%, while that in ore sample A with the smallest fractal dimension was only 4%.

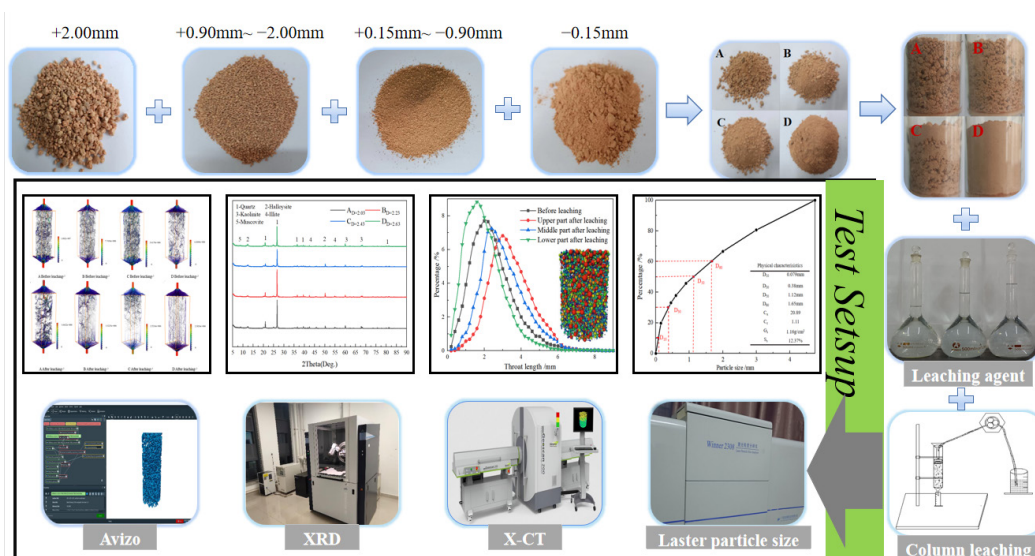


Figure 3. Preparation of experimental samples, including experimental equipment and test outcomes.

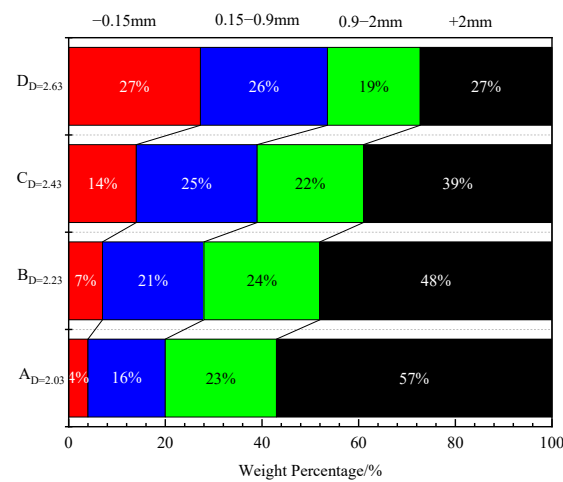


Figure 4. Mass percentage of four kinds of ores samples within each particle size range.

2.3. Experimental Methods

2.3.1. Column Leaching Experiments

The column experiments were completed by the column experimental device, including an iron frame and a glass permeation column with a diameter of 50 mm, as shown in Figure 3. Firstly, the prepared ore samples were put into the glass column layer by layer and were compacted by using a tamping rod. Secondly, one piece of 1 cm-thick filtering paper was laid on the top of the ore samples to make the solution penetrate the samples evenly [22]. In addition, 0.2 mol/L ammonium sulfate solution was slowly injected into the samples to form a stable liquid column on the top of the ore samples. Peristaltic pumps were used to maintain a constant injection rate. Finally, the experimental samples were scanned using X-ray computed tomography (X-CT) equipment after leaching.

2.3.2. Construction of Three-Dimensional Pore Structure

The 3D CT scanner (Geoscan200) was adopted for scanning four kinds of ore samples before and after leaching. Its scanning speed was 1 m/h and its maximum spatial resolution was 56.05 μm . It took approximately three minutes to complete the scanning of the entire ore sample. Firstly, 500 images were obtained by scanning the ore sample. Each image contained 1920 \times 1920 pixels. Then, the images were imported into Avizo software. In addition, the image was clipped, filtered and denoised to enhance the structural characteristics of the ore sample. In addition, the threshold segmentation algorithm was used to segment the pores and particles. The pores were marked. Eventually, the pore volume, shape and other characteristic parameters of the pore structure were analyzed by using the label analysis algorithm. The construction process of the three-dimensional pore structure model was shown in Figure 5.

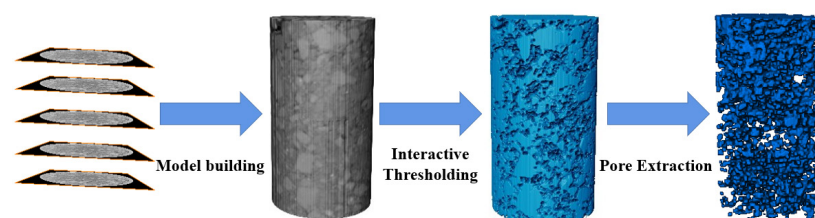


Figure 5. The construction process of the three-dimensional pore structure model.

2.3.3. Numerical Simulation Analysis

The numerical simulation analysis on the various characteristics of the solution seepage path and the pore pressure was completed using Avizo software. Firstly, the constructed three-dimensional pore structure models, before and after leaching, were taken as

the research objects, which were then imported into the absolute permeability experiment simulation module (Avizo XLab Hydro Extension) in Avizo 2019.1 software. Then, an input pressure of 10 MPa was set at the inlet end of the established models. An output pressure of 0 MPa was set at the outlet end. The inlet and outlet flow remained unchanged, and the viscosity of the water flow was 0.8 Pa·s. Finally, a numerical simulation calculation was carried out to explore the variation law of the solution seepage path and the pore pressure, as shown in Figure 3.

3. Results

3.1. Evolution Characteristics of the Pore Structure of Rare Earth Ores during Leaching

The pore structure directly affected the seepage diffusion movement of the solution and determined the leaching velocity of the solution [11]. It included two parts: pore and pore throat. The pores could be used as the container for storing solution, while the pore throat was a bridge passage used to connect pores. For the weathered rare earth ores, the pore structure characteristics have changed significantly after leaching. The direction slices of pore structures A and C are shown in Figure 6. Therefore, the various rules of the characteristic parameters of the pore and pore throat were analyzed to reveal the mechanism for the decline of the leaching velocity of weathered rare earth ores in the leaching process.

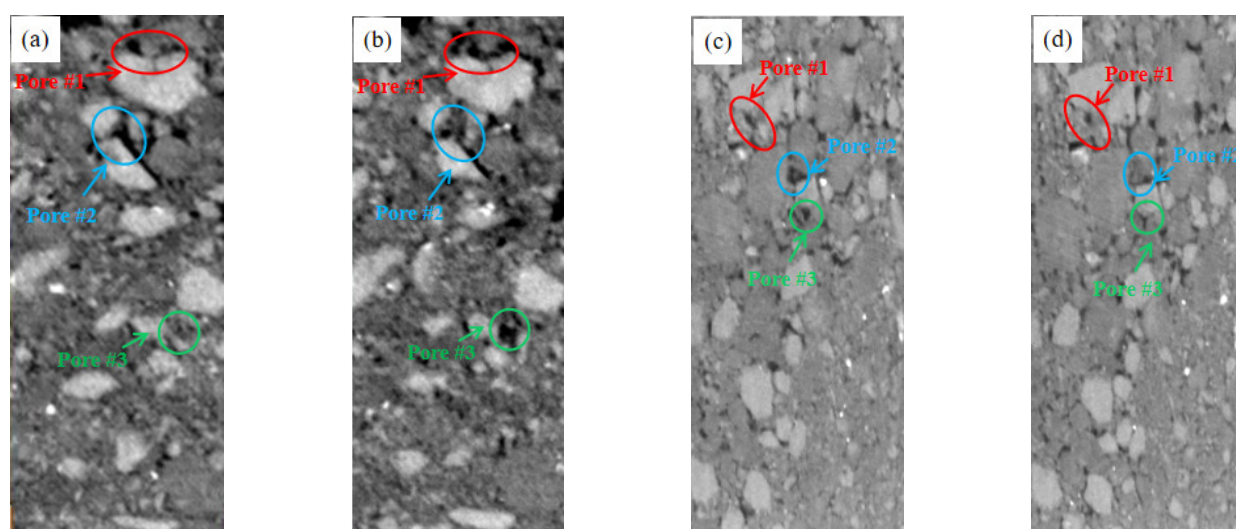


Figure 6. Slice images of the ore sample A and C before and after leaching. (a) $A_{D=2.03}$ Before leaching; (b) $A_{D=2.03}$ After leaching; (c) $C_{D=2.43}$ Before leaching; (d) $C_{D=2.43}$ After leaching.

3.1.1. Evolution Law of Pore Characteristic Parameters

(1) Pore volume

The pore volume represented the ability to store liquid, which controlled the pore water pressure and directly affected the seepage diffusion velocity [23]. The distribution rules of the pore volume of ore samples at different depths before and after leaching were obtained through statistical analysis, as shown in Figure 7.

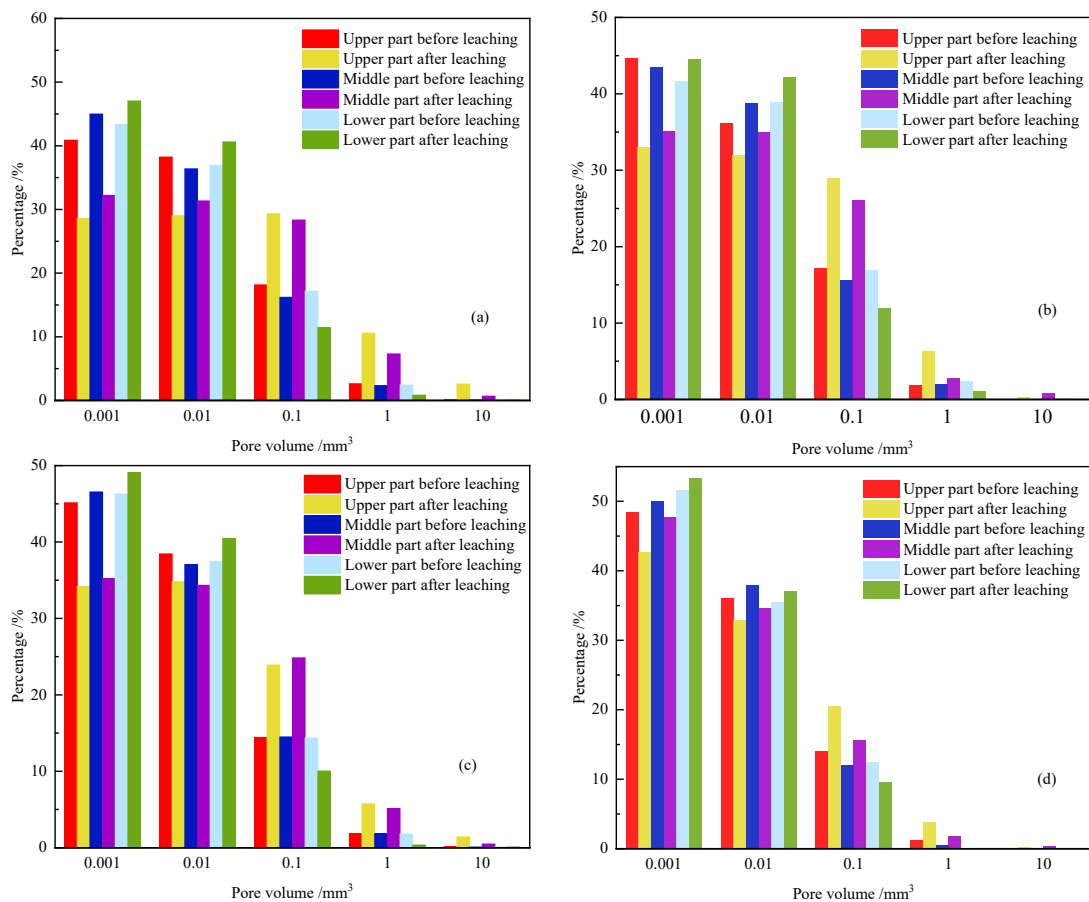


Figure 7. Distribution rules of the pore volume of ore samples at different depths before and after leaching. (a) $A_D=2.03$; (b) $B_D=2.23$; (c) $C_D=2.43$; (d) $D_D=2.63$.

Figure 7 showed that distribution characteristics of the pore volume at the upper, middle and lower heights of the samples before leaching were basically the same, while the number of pores decreased gradually with the increase of the pore volume. It indicated that the pore structure distribution of the ore samples before leaching was very uniform. However, the number of pores in ore samples at different depths changed during leaching. The proportion of the number of pores with a volume of less than 0.01 mm³ in the upper and middle samples decreased, while the pore quantity with that in the lower samples increased. On the contrary, the number of pores with a volume of more than 0.01 mm³ in the upper and middle samples increased while the pore quantity with that in the lower samples decreased. It may be because of the migration of fine particles in the upper samples under the effect of solution seepage, resulting in the continuous expansion of some large pores and the penetration of small pores into larger pores [24]. With the gradual migration of fine particles to the bottom, some large pore channels were blocked or divided into small pores by fine particles, leading to the reduction of the amount of solution stored. It further reduced the leaching velocity. In addition, the change rate of the pore volume of the four kinds of ore samples was in the order of $A > B > C > D$. That is, it increased with the increase of the fractal dimension of the particle gradation. For example, the proportion of the number of pores with a volume of greater than 0.01 mm³ in the upper and middle samples A, B, C and D increased by 103.28%, 89.16%, 86.98% and 59.04%, respectively, while that in the lower samples decreased by 37.34%, 35.60%, 32.29% and 23.86%, respectively. This was because with the increase of fractal dimension, the content of fine particles became more and more, the number of small pores was increasing and the migration capacity of fine particles in the upper part of the ore samples was weakening, which reduced the damage degree of the pore structure.

(2) Pore connectivity

Pores were divided into isolated pores and connected pores. The pore connectivity represented the percentage of the connected pores. In the process of solution seepage, the pore connectivity could directly reflect the leaching velocity of the solution. The greater the pore connectivity, the faster the flow speed of the solution [25]. The connectivity could be obtained by the ratio of the total volume of the connected pores to the total volume of samples, as shown in Table 1.

Table 1. Pore connectivity of four kinds of ore samples.

	A		B		C		D	
	Before Leaching	After Leaching						
Upper part	0.0658	0.0958	0.0587	0.0792	0.0375	0.0457	0.0164	0.0186
Middle part	0.0683	0.0522	0.0605	0.0476	0.0347	0.0282	0.0145	0.0125
Lower part	0.0713	0.0443	0.0578	0.0373	0.0357	0.0242	0.0157	0.0118

Table 1 illustrated that the average pore connectivity of ore samples A, B, C and D before leaching was 0.0685, 0.0590, 0.0359 and 0.01553, respectively, while that of them after leaching was reduced to 0.0641, 0.0547, 0.0327 and 0.0143, respectively. It indicated that the pore connectivity of the ore samples decreased with the increase of the fractal dimension. The main reason was that the ore samples with larger fractal dimensions had fewer macropores and more small pores, leading to larger pore tortuosity and smaller pore connectivity [26]. Compared with that before leaching, the pore connectivity of the upper ore samples A, B, C and D increased by 45.48%, 34.99%, 21.79% and 13.9%, respectively, while that of the lower ore samples decreased by 37.82%, 35.45%, 32.43% and 25.29%, respectively. The reduction rate of the lower samples was higher than that of the middle samples. This was because the pore in the middle and lower ore samples was blocked due to particle migration. The blockage degree of the lower samples was higher than that of the middle samples. It was consistent with the variation law of the change rate of the pore volume. In addition, Table 1 demonstrated that the change rate of the pore connectivity of the ore samples after leaching decreased with the increase of the fractal dimension. This was because the more fine the particles, the smaller the change degree of the pore structure, resulting in the decrease of the change rate of pore connectivity.

(3) Fractal dimension of the pore shape

The pore shape characteristics could reflect the spatial geometric complexity of the pores, which directly determined the seepage direction of the solution and affected the seepage characteristics of the ore samples. Pore fractal dimension was usually used to quantitatively describe it. The spatial complexity of the pore structure increased with the fractal dimension of the pore shape decreasing [14]. The change rule of the pore shape was obtained by fractal dimension in this paper, as shown in Figure 8. Where A_u , A_m , A_b , B_u , B_m , B_b , C_u , C_m , C_b , D_u , D_m and D_b represented the upper, middle and lower parts of the four kinds of ore samples, A, B, C and D, respectively.

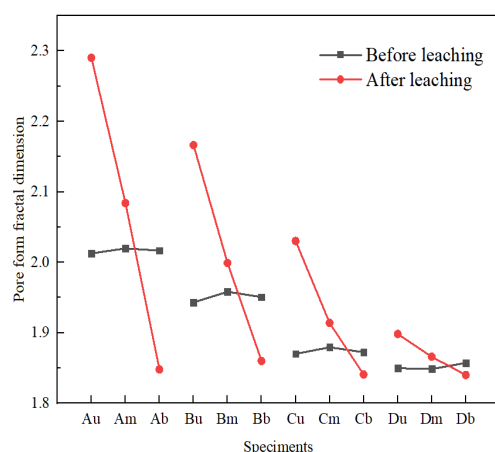


Figure 8. Change rules of fractal dimension of pore shape.

Figure 8 showed that the fractal dimensions of the pore shape of the ore samples at different depths before leaching were basically the same, which decreased with the increase of the fractal dimension of particle gradation. It indicated that the particle size distribution of ore samples before leaching was very uniform, but the complexity of the pore shape increased with the increase of the fractal dimension. This was mainly because ore samples with a high coarse particle content had a large number of macropores and a simple pore structure. In addition, the fractal dimension of the pore shape of the upper and middle ore samples increased while that of the lower ore samples decreased. It demonstrated that the pore shape had changed under the effect of solution seepage during leaching. The pore shape structure in the upper ore samples became more complex with the increase in depth. It was because the migration of the fine particles in the upper ore sample during leaching was more obvious while the deposition of the lower ore sample was more visible. It made the pore shape structure of the upper ore sample simple while that of the lower ore sample became more complex. At the same time, it could be seen from Figure 8 that the fractal dimension of the pore shape of ore sample A changed most obviously, which was because the content of fine particles in the ore sample A was the least and the migration of the particles in the upper samples was the largest, resulting in the largest proportion of the volume and quantity of large pores in the upper ore samples. It made the pore shape structure in the upper part of the samples the simplest [27].

(4) Pore length and width

The pore size could indirectly reflect the porosity of ore samples [28]. This paper described the pore size of ore samples by pore length and width. The variation rules of pore length and width of four kinds of ore samples with different depths through a statistical analysis were shown in Figures 9 and 10, respectively.

Figure 9 demonstrated that the pore length of ore samples A, B, C and D before leaching was mainly 1–5 mm. The number of longer pores decreased with the increase of the fractal dimension of particle gradation. It indicated that the pore length was determined by the number of spatial structures of coarse particles. The stronger the skeleton effect of the coarse particles was, the longer the pore length. It indirectly confirmed that the change law of pore volume was correct. In addition, the pore length of ore samples changed during leaching. The pore length in the upper and middle ore samples increased continuously while that in the lower ore samples gradually decreased. At the same time, the number of pores in the upper and middle ore samples decreased first and then increased, while the pore quantities in the lower ore samples increased first and then decreased. In addition, the change degree of the pore length increased with the decrease of the fractal dimension of particle gradation. For example, the change rate of the number of pores with pore lengths less than 2 mm in ore samples A, B, C and D were 41.81%, 28.4%, 25.61% and 16.66%, respectively. This was due to the particle migration of fine particles under the

combined effect of seepage force, gravity and other factors, which led to the penetration and expansion of upper and middle pores, increasing the proportion of longer pores while the blockage of lower pores led to an increase in the proportion of shorter pores. This phenomenon was the most obvious, especially for ore samples with a small content of fine particles [18].

It could be seen from Figure 10 that most of the pore widths of ore samples A, B, C and D were less than 2 mm, accounting for 85.23%, 89.06%, 92.03% and 94.18%, respectively. It showed that the number of pores with pore widths less than 2 mm increased with the increase of fractal dimension, which was mainly because the number of small pores of ore samples with large fractal dimensions accounted for more. The pore widths of ore samples had changed after leaching. The percentage of pores in the upper and middle samples with pore widths less than 2 mm decreased while those in the lower samples increased. At the same time, the percentage of pores with upper pore widths less than 2 mm had changed by 8.93%, 7.41%, 5.80% and 3.35%, respectively. On the contrary, the number of pores with a pore width greater than 2 mm increased, while that with a pore width greater than 2 mm decreased. This was consistent with the change rule of pore length and pore volume.

According to the variation law of the pore length and the pore width, the pore size changed during leaching. The change rate of the pore length after leaching was higher than that of the pore width. That is, the ratio of pore length to width gradually decreased, which indicated that the pore shape gradually evolved from blocky to banded under the seepage of the leaching solution. This caused a preferential seepage phenomenon in ore samples [22], which was not conducive to the seepage diffusion of the leaching solution and affected the leaching efficiency of the rare earth ores.

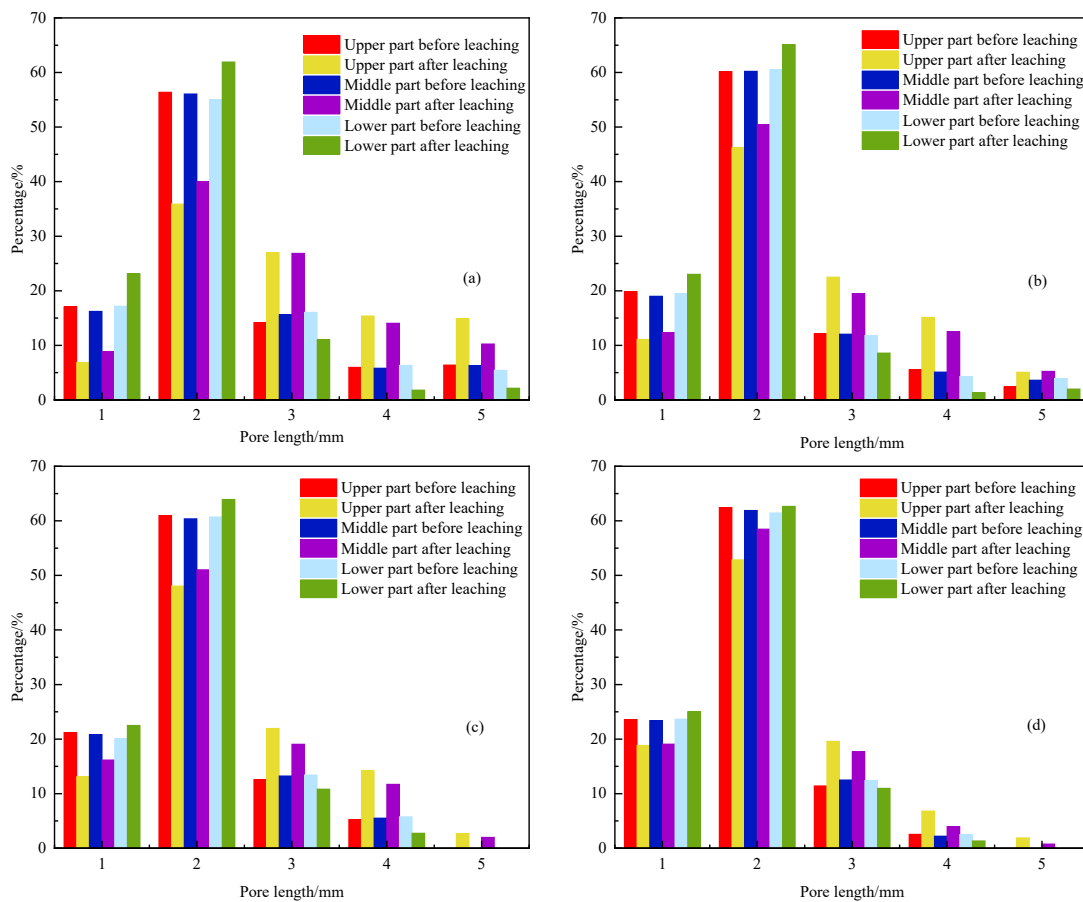


Figure 9. Variation rules of the pore length of four kinds of ore samples with different depths. (a) $A_D=2.03$; (b) $B_D=2.23$; (c) $C_D=2.43$; (d) $D_D=2.63$.

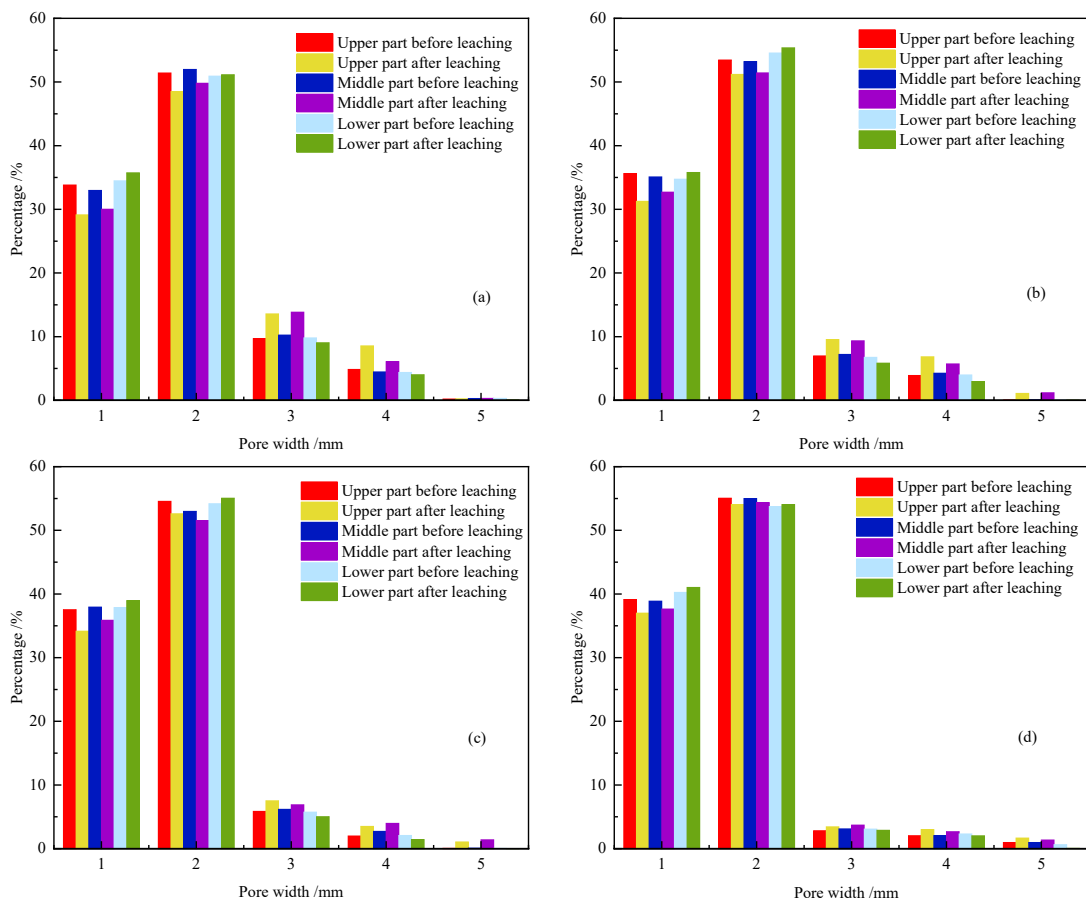


Figure 10. The variation rules of the pore width of four kinds of ore samples with different depths. (a) $A_D=2.03$; (b) $B_D=2.23$; (c) $C_D=2.43$; (d) $D_D=2.63$.

(5) Two-dimensional porosity

Two-dimensional porosity could be used to describe the permeability of ores [29]. Two-dimensional porosity referred to the percentage of pixels in the white area of an image to the total pixels of the entire image, which was the ratio of pore voxels to total pixels. Based on the principle of porosity calculation, 500 images of each ore sample were statistically analyzed. The curves of two-dimensional porosity along the height of ore samples before and after leaching are shown in Figure 11.

Figure 11 implied that the two-dimensional porosity of ore samples with different depths before leaching was basically the same, with an average porosity of 8.65%, 6.85%, 5.06% and 2.54%, respectively. This again illustrated that the ore samples before leaching were evenly distributed. The porosity of the ore samples with fewer fine particles and higher coarse particles was larger. Compared with that before leaching, the average two-porosity of the four kinds of ore samples during leaching increased. The porosity of the upper ore samples after leaching was significantly higher than that of the lower ore samples, with the difference ratio reaching 25.86%, 23.62%, 20.95% and 5.07%, respectively. This was mainly because the fine particles migrated downward under the seepage pressure of the leaching solution and their gravity, increasing the pore size of the upper ore sample and the increase of the pore change rate. At the same time, for ore samples with small fractal dimensions, the higher the content of coarse particles, the higher the mobility of the fine particles. This led to a more obvious porosity change [30].

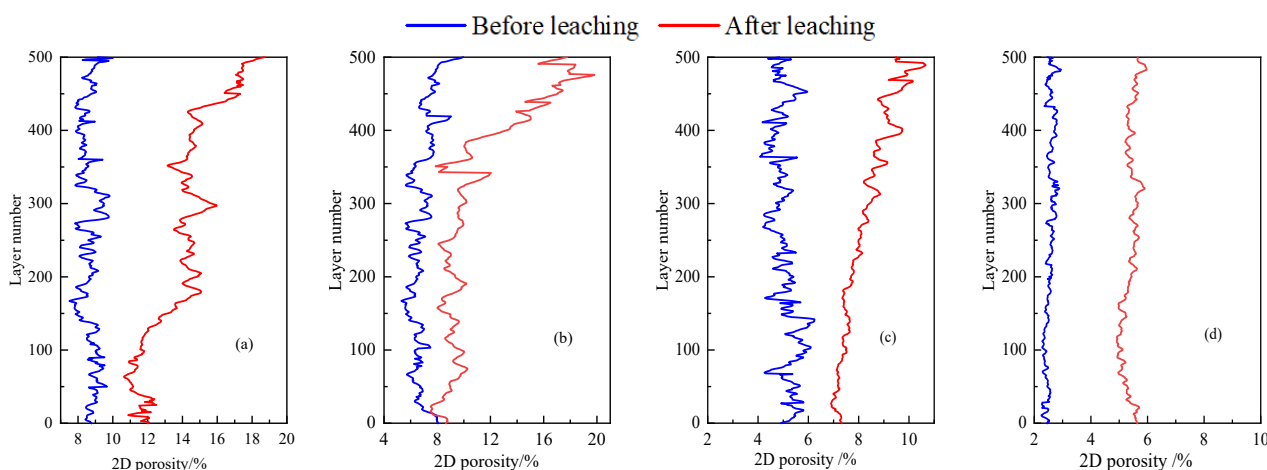


Figure 11. Two-dimensional porosity of ore samples in the vertical direction. (a) $A_{D=2.03}$; (b) $B_{D=2.23}$; (c) $C_{D=2.43}$; (d) $D_{D=2.63}$.

3.1.2. Evolution Law of Pore Throat Characteristic Parameters

As the connecting channel between pores, the pore throat directly affected the seepage diffusion movement of the leaching solution between pores [23]. The characteristic parameters of the pore throat mainly included pore throat length and pore throat radius. The pore throat length controlled the maximum volume of solution that can be stored in the pore throat channel. The pore throat radius determined the percolation velocity of the leaching solution. Therefore, this paper mainly focuses on the statistical analysis of the variation law of pore throat characteristic parameters (pore throat length and pore throat radius) of the ore samples at different depths in the leaching process.

(1) Pore throat length

Figure 12 showed that the number of pore throats of ore samples increased rapidly at first and then decreased fast with the increase of the pore throat length, which was mainly between 2 mm and 4 mm. The average throat length of ore samples A, B, C and D before leaching was 2.58 mm, 2.54 mm, 2.44 mm and 2.12 mm, respectively. It indicated that the average pore throat length of the ore samples decreased with the increase of the fractal dimension of particle gradation, which was mainly because ore samples with small fractal dimensions have larger pore sizes, making the connecting passage (throat length) between them longer. In addition, the proportion of the pore throat length of the ore samples after leaching has changed. The average pore throat length of the upper and middle ore samples became longer while that of the lower ore samples became shorter. For example, the proportion of the pore throat length of less than 2 mm in the four kinds of upper ore samples A, B, C and D decreased by 79.05%, 71.47%, 54.93% and 47.43%, respectively, while that of the lower ore samples increased by 45.28%, 40.02%, 26.38% and 14.86%, respectively. However, the number of pore throats larger than 4 mm in the upper ore samples increased by 148.48%, 124.05%, 111.73% and 81.49%, respectively, while those in the lower ore samples decreased by 49.17%, 37.09%, 24.71% and 21.56%, respectively. This was mainly because some small particles were carried downward by the leaching solution during leaching, resulting in the reduction of the number of small pores in the upper ore samples and the increase in the number of large pores. This made the length of the pore throat longer. For the lower ore samples, the large pores in the inner part became small pores due to blockage, resulting in the increasing number of small pores and the shortening of the average pore path between the pores [31].

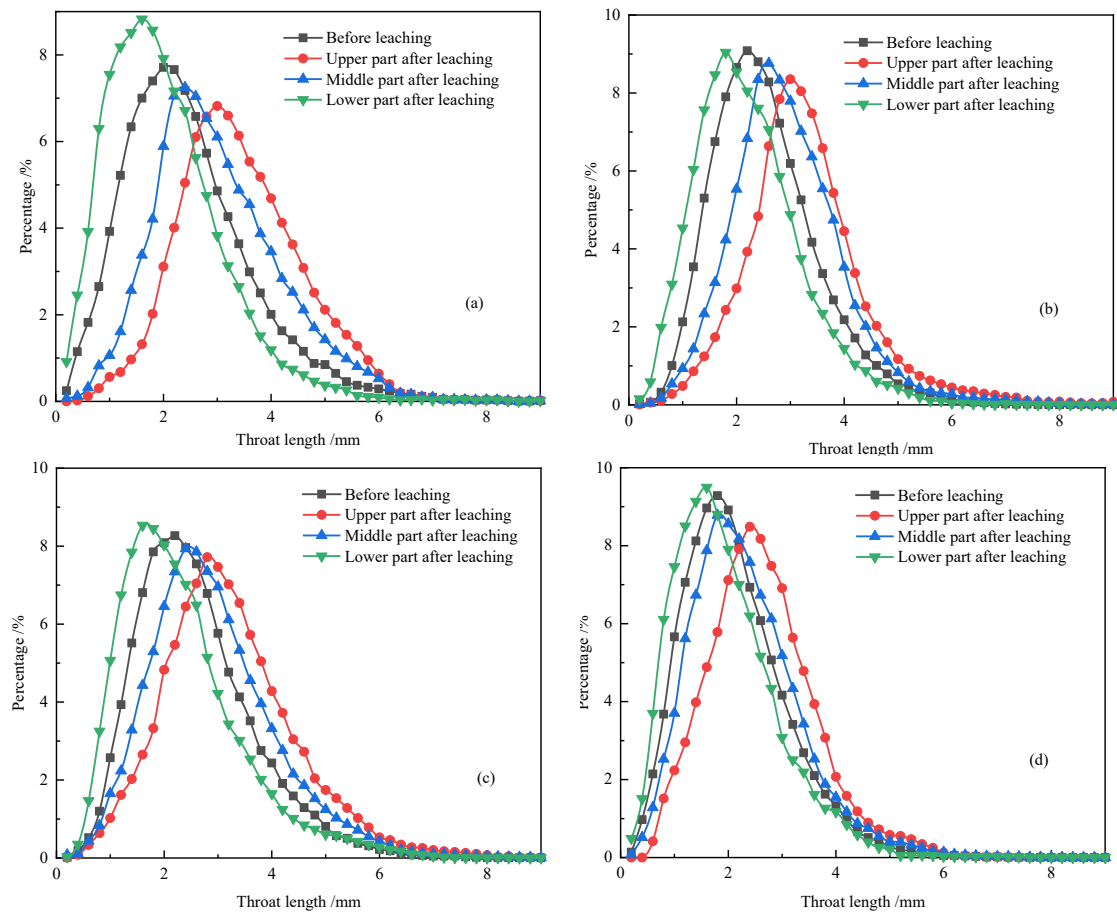


Figure 12. Distribution curves of the pore throat length. (a) $A_{D=2.03}$; (b) $B_{D=2.23}$; (c) $C_{D=2.43}$; (d) $D_{D=2.63}$.

(2) Pore throat radius

It can be seen from Figure 13 that the pore throat radius of four kinds of ore samples before leaching was mainly distributed between 0.05 mm and 0.80 mm, with average pore throat radii of 0.803 mm, 0.753 mm, 0.634 mm and 0.547 mm, respectively. After leaching, the average pore throat radius of the upper ore samples A, B, C and D increased to 0.995 mm, 0.921 mm, 0.723 mm and 0.605 mm, respectively, while that of the lower ore samples decreased to 0.529 mm, 0.515 mm, 0.495 mm and 0.468 mm, respectively. It showed that the average pore throat radius of ore samples has changed. For example, the proportion of the upper ore samples A, B, C and D with a pore radius less than 0.8 mm decreased by 28.07%, 24.44%, 20.95% and 18.46%, while those of the lower part increased by 18.52%, 14.98%, 10.62% and 6.08%, respectively. At the same time, the proportion of the upper ore samples with a pore radius of more than 1.2 mm increased by 148.02%, 122.84%, 88.08%, 69.94%, while those of the lower part decreased by 67.72%, 41.21%, 21.23%, and 17.08%, respectively.

According to the comprehensive analysis of the variation law of characteristic parameters of the pore structure, it was known that the change rule of characteristic parameters of the pore throat was consistent with the evolution law of the pore characteristic parameters. It was mainly because the pore structure characteristics were controlled by pore throats and pores cooperating, which affected the seepage diffusion process of the leaching solution. In addition, it also showed that the characteristic parameters of the pore structure between ore particles were constantly weakening during leaching. Accordingly, the evolution law of the characteristic parameters of pores and pore throats could well reveal the weaken-

ing mechanism of the leaching seepage velocity of the weathered rare earth ore from the perspective of a solid phase.

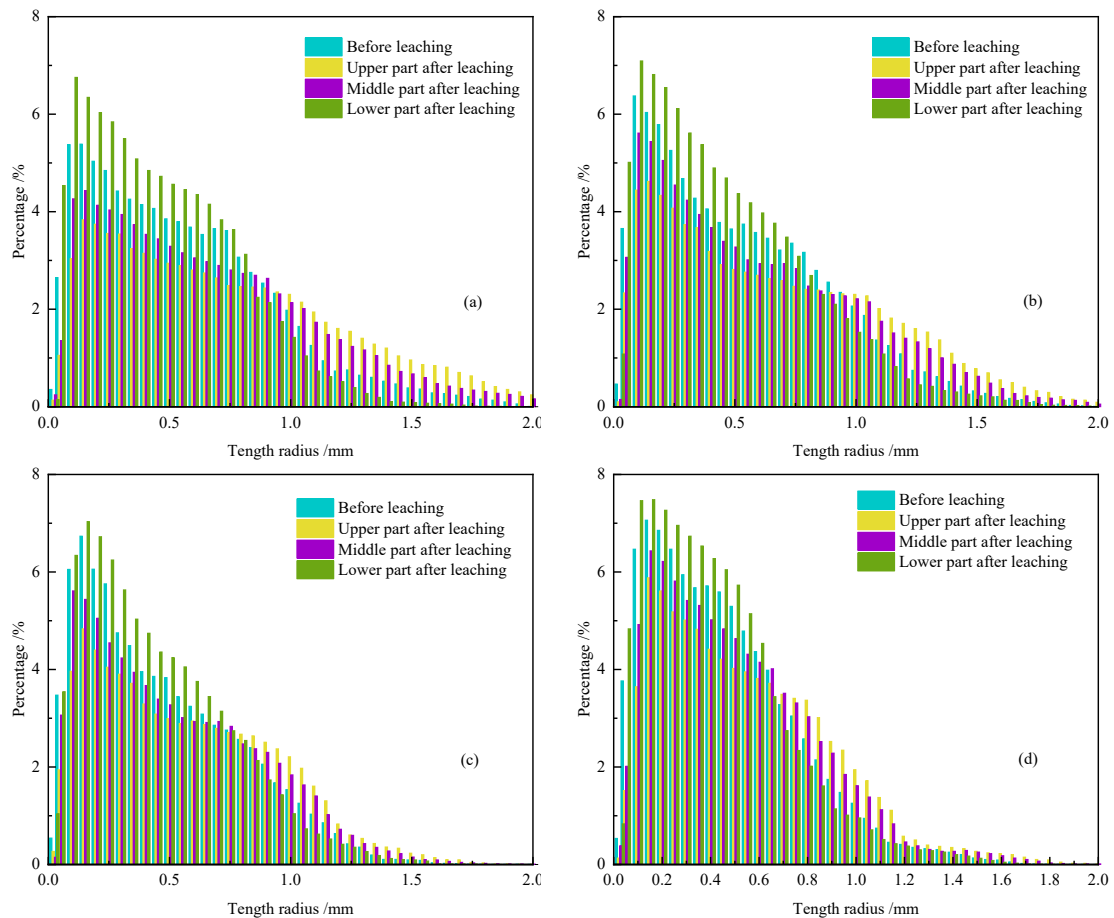


Figure 13. Distribution curves of the pore throat radius. (a) $A_D=2.03$; (b) $B_D=2.23$; (c) $C_D=2.43$; (d) $D_D=2.63$.

3.2. Evolution Characteristics of the Leaching Solution

3.2.1. Variation Law of Seepage Path of the Solution

The leaching process of the rare earth was carried out under the coupling effect of the solid and liquid phases. Clarifying the variation law of the solution seepage path was helpful to reveal the weakening mechanism of the leaching seepage velocity of the weathered rare earth ore from the perspective of a liquid phase. Therefore, the three-dimensional seepage path and average seepage velocity through numerical simulation were obtained in this paper, as shown in Figure 14 and Table 2, respectively.

Table 2. Seepage velocity of ore samples at different depths after leaching.

	A (10^{-6} m/s)	B (10^{-6} m/s)	C (10^{-6} m/s)	D (10^{-6} m/s)
Upper part	2.43	2.24	1.78	1.57
Middle part	2.12	1.69	1.27	1.11
Lower part	1.62	1.47	1.03	0.88
Average seepage velocity	1.82	1.61	1.26	1.19

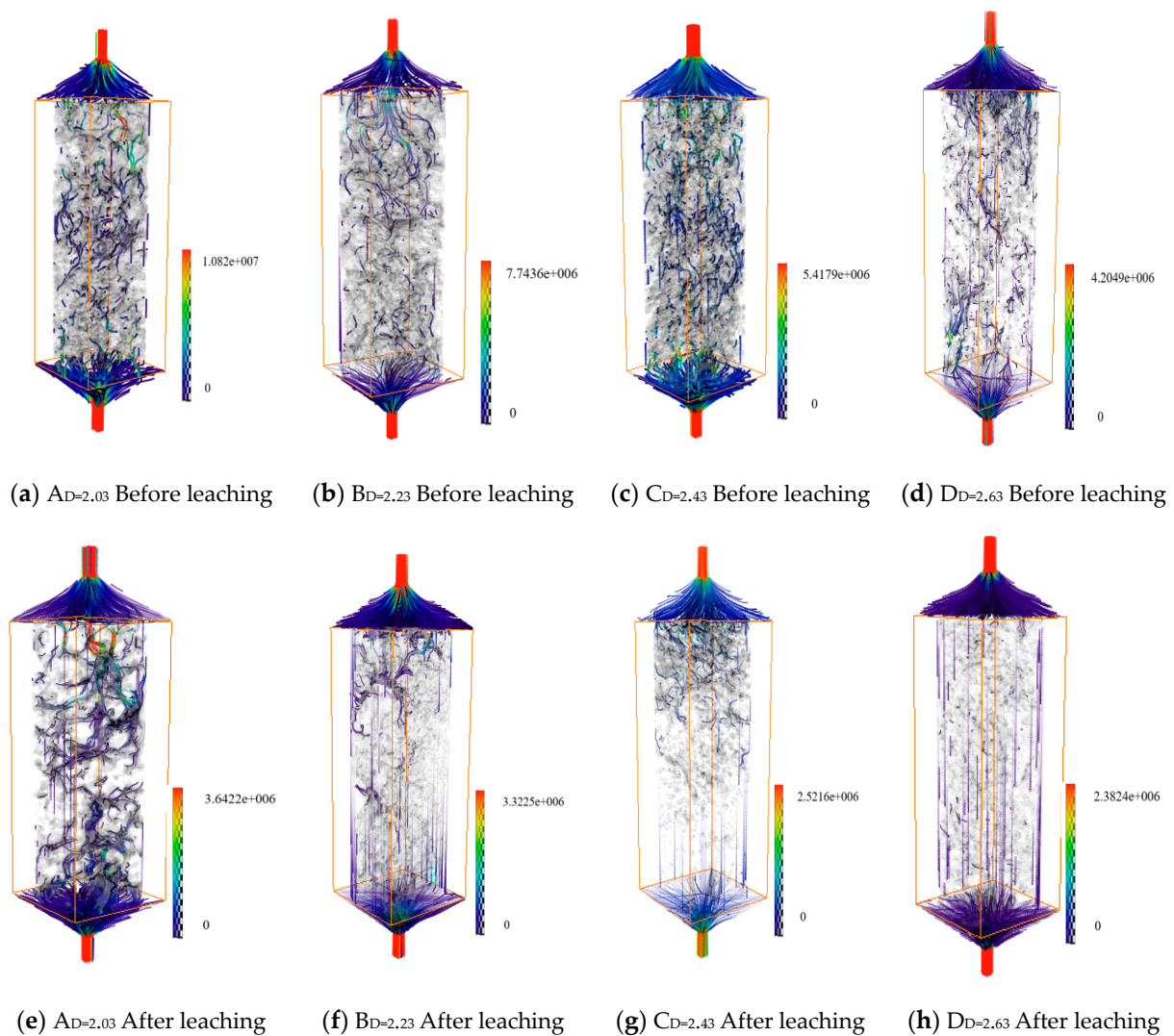


Figure 14. Distribution characteristics of the seepage path of the solution in ore samples during leaching. (a) $A_{D=2.03}$ Before leaching; (b) $B_{D=2.23}$ Before leaching; (c) $C_{D=2.43}$ Before leaching; (d) $D_{D=2.63}$ Before leaching; (e) $A_{D=2.03}$ After leaching; (f) $B_{D=2.23}$ After leaching; (g) $C_{D=2.43}$ After leaching; (h) $D_{D=2.63}$ After leaching.

Figure 14 illustrated that both the solution seepage path and the seepage velocity of ore samples before leaching were evenly distributed. The seepage velocity of ore samples A, B, C and D was 5.41×10^{-6} m/s, 3.87×10^{-6} m/s, 2.71×10^{-6} m/s and 2.1×10^{-6} m/s, respectively. It demonstrated that the seepage velocity decreased with the increase of the fractal dimension. This was consistent with the relationship between the pore structure characteristics and fractal dimension in 3.2, which also indicated that the seepage velocity of the solution was mainly controlled by pore structure characteristics [32]. In addition, the seepage path of the solution in ore samples changed after leaching. The streamline of the upper and middle ore samples was concentrated, while the streamline density of the lower ore samples was small and even interrupted. This was mainly due to the migration of fine particles. The migration of fine particles in the upper ore samples led to a simpler pore structure and wider effective pore channels, which enhanced the connectivity of some of the pores. However, the migration of fine particles in the lower ore sample caused the pore structure to become complex and some pore channels to be blocked, which reduced some pore connectivity. It produced preferential seepage, which became weaker with the increase of the fractal dimension of particle gradation. This was not conducive to solution seepage in the rare earth ores. At the same time, the average seepage velocity of the four

kinds of ore samples decreased to 1.82×10^{-6} m/s, 1.61×10^{-6} m/s, 1.26×10^{-6} m/s and 1.19×10^{-6} m/s, respectively. In addition, the seepage velocity of the solution during leaching gradually decreased with the increase of the ore sample depth (see Table 2). For example, the seepage velocity of solution in ore samples A, B, C and D decreased from 2.43×10^{-6} m/s to 1.62×10^{-6} m/s, from 2.24×10^{-6} m/s to 1.47×10^{-6} m/s, from 1.78×10^{-6} m/s to 1.03×10^{-6} m/s and from 1.57×10^{-6} m/s to 0.88×10^{-6} m/s, respectively.

3.2.2. Variation Characteristics of the Pore Pressure

The pore pressure could well describe the difficulty and simplicity of solution seepage [33]. Simulation calculation of the solution seepage was conducted for ore samples before and after leaching. The distribution characteristics of the pore pressure of the ore samples were obtained, as shown in Figure 15 and Table 3, respectively.

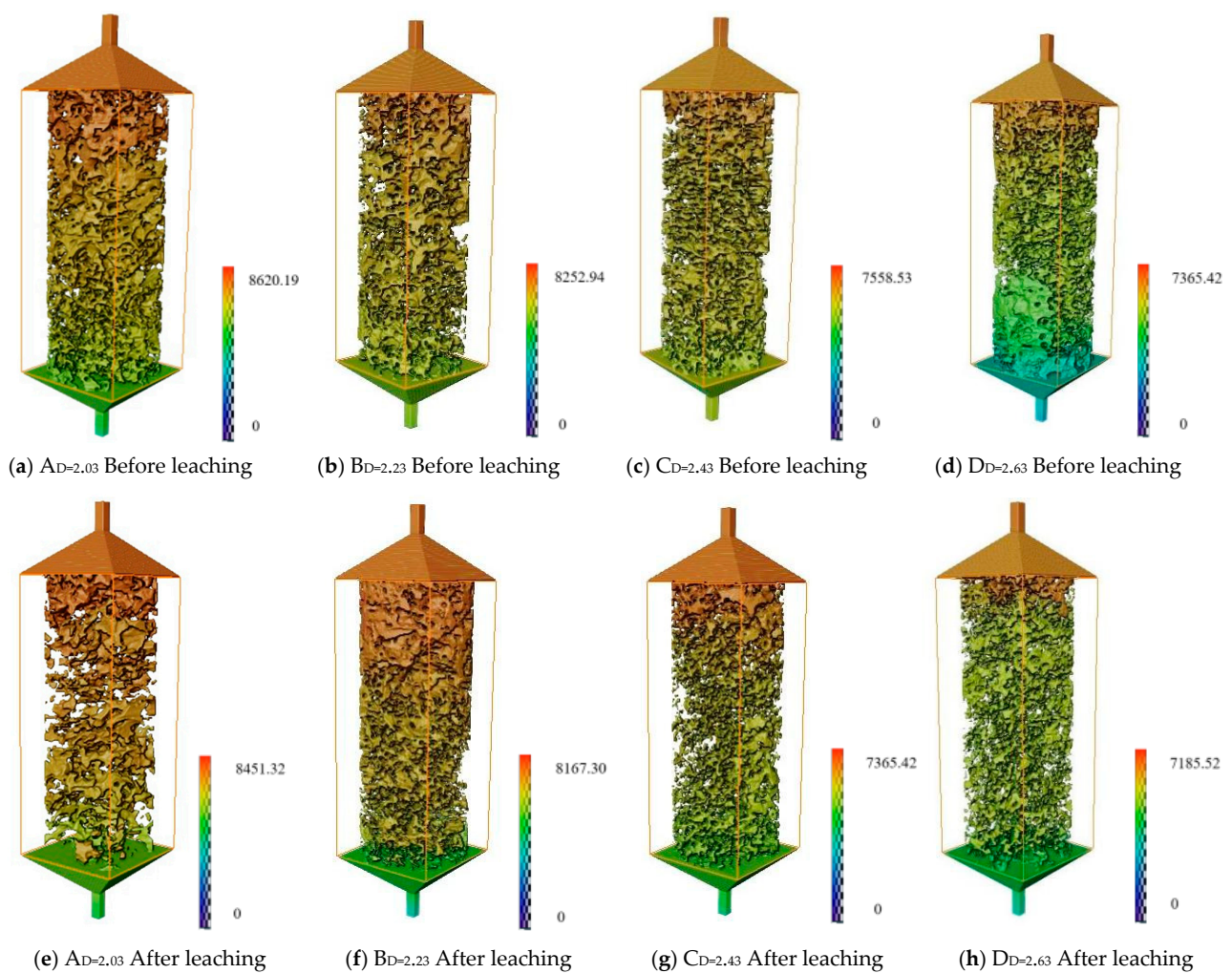


Figure 15. Distribution diagrams of pore pressure of ore samples. (a) $A_{D=2.03}$ Before leaching; (b) $B_{D=2.23}$ Before leaching; (c) $C_{D=2.43}$ Before leaching; (d) $D_{D=2.63}$ Before leaching; (e) $A_{D=2.03}$ After leaching; (f) $B_{D=2.23}$ After leaching; (g) $C_{D=2.43}$ After leaching; (h) $D_{D=2.63}$ After leaching.

Table 3. Pore pressure of ore samples at different depths after leaching.

	A/Pa	B/Pa	C/Pa	D/Pa
Upper part	4253.82	4172.34	3724.92	3621.05
Middle part	4176.37	4083.25	3682.84	3587.15
Lower part	4013.29	3972.71	3624.28	3559.93
Average pore pressure	4106.18	4043.37	3636.29	3507.63

Figure 15 showed that the maximum pore pressure occurred at the solution inlet. The pore pressure also decreased gradually along the solution seepage direction in ore samples. It indicated that the solution gradually flowed and diffused along the vertical direction, which was due to the combined effect of the hydraulic gradient of the upper solution, matrix suction and gravity. However, this phenomenon was also affected by the pore structure characteristics between ore particles. For example, the average pore pressure of the four groups of ore samples before leaching was 4310.095 Pa, 4225.660 Pa, 3779.265 Pa and 3637.06 Pa, respectively. It was because both the pore structure and the connectivity of ore samples became complex with the increase of the fractal dimension of particle gradation, leading to a continuous decrease of pore pressure. In addition, the average pore pressure of ore samples after leaching was reduced to 4106.18 Pa, 4043.37 Pa, 3636.29 Pa and 3507.63 Pa, respectively. This was one of the reasons why the seepage velocity of the solution decreased. In addition, it can be seen from Figure 15 and Table 3 that the pore pressure of the upper and middle ore samples after leaching was significantly higher than that of the lower ore samples. This was because of the downward migration of fine particles [34], the pore size of the upper part of ore samples became larger, the pore structure became simpler and the content of the solution stored in the pore became more, leading to the increase of its pore pressure. However, due to the blockage of fine particles in the lower part of the ore sample, the pore size became smaller, the pore structure got more complex and the amount of solution flowing through the pore channel became less, making the pore pressure smaller. This was consistent with the variation law of the characteristic parameters of the pore structure.

4. Conclusions

- (1) Compared with those before leaching, the pore characteristic parameters of ore samples at different depths after leaching had changed significantly. Both the pore quantities with pore volume less than 0.01 mm^3 and a pore radius of less than 0.8 mm increased for the lower ore samples while that of the upper and middle ore samples reduced. At the same time, the pore connectivity, the fractal dimension of the pore shape and the ratio of pore length to width and pore length in the lower ore samples decreased.
- (2) The solution seepage path and the pore pressure of ore samples during leaching were weakened. After leaching, the solution paths of the upper and middle ore samples were concentrated, while those of the lower samples were few, even interrupted. In addition, the average pore pressure reduced to 4106.18 Pa, 4043.37 Pa, 3636.29 Pa and 3507.63 Pa, respectively. However, the pore pressure of the lower ore samples showed the highest reduction compared with the upper and middle ore samples. The research results not only reveal the continuously weakening mechanism of the leaching velocity of weathered rare earth ores with the increase of ore burial depth, but also help to enrich the basic theory on the heap leaching of weathered rare earth ores.

Author Contributions: Writing—original draft preparation, D.L.; methodology, W.Y.; writing—review and editing, Z.Z.; data curation, W.G.; supervision, R.C.; funding acquisition, D.L. and Z.Z. All authors have read and agreed to the published version of the manuscript.

Funding: All sources of funding for the study were supported by the National Natural Science Foundation of China (No: 52174258, 92162109, 52222405 and 52004184).

Data Availability Statement: Not applicable.

Acknowledgments: All the experimental labs were supported by the Wuhan Institute of Technology.

Conflicts of Interest: The authors declare no conflict of interest.

References

1. Chi, R.A.; Tian, J.; Li, Z.J.; Peng, C.; Wu, Y.X.; Li, S.R.; Wang, C.W.; Zhou, Z.A. Existing State and Partitioning of Rare Earth on Weathered Ores. *J. Rare Earths* **2005**, *23*, 756–759. [\[CrossRef\]](#)
2. Zhang, Z.Y.; He, Z.Y.; Xu, Z.G.; Yu, J.X.; Zhang, Y.F.; Chi, R.A. Rare earth partitioning characteristics of China rare earth ore. *Chin. Rare Earths* **2016**, *37*, 127–133. [\[CrossRef\]](#)
3. Liu, D.F.; Zhang, Z.Y.; Chi, R.A. Seepage mechanism during in-situ leaching process of weathered crust elution-deposited rare earth ores with magnesium salt. *Physicochem. Probl. Miner. Process.* **2020**, *56*, 350–362. [\[CrossRef\]](#)
4. Zhang, Z.Y.; He, Z.Y.; Yu, J.X.; Xu, Z.G.; Chi, R.A. Novel solution injection technology for in-situ leaching of weathered crust elution-deposited rare earth ores. *Hydrometallurgy* **2016**, *164*, 248–256. [\[CrossRef\]](#)
5. Moldoveanu, G.; Papangelakis, V. Chelation-Assisted Ion-Exchange Leaching of Rare Earths from Clay Minerals. *Metals* **2021**, *11*, 1265. [\[CrossRef\]](#)
6. Agatzini-Leonardou, S.; Oustadakis, P.; Dimaki, D.; Zafiratos, J.; Tsakiridis, P.; Karidakis, T.; Frogoudakis, E.; Drougas, J. Heap Leaching of Greek Low-Grade Nickel Oxide Ores by Dilute Sulphuric Acid at a Pilot-Plant Scale. *Mater. Proc.* **2021**, *5*, 65. [\[CrossRef\]](#)
7. He, Z.Y.; Zhang, Z.Y.; Yu, J.X.; Xu, Z.G.; Chi, R.A. Process optimization of rare earth and aluminum leaching from weathered crust elution-deposited rare earth ore with compound ammonium salts. *J. Rare Earths* **2016**, *34*, 413–419. [\[CrossRef\]](#)
8. Xiao, Y.F.; Feng, Z.Y.; Hu, G.H.; Huang, L.; Huang, X.W.; Chen, Y.Y.; Long, Z.Q. Reduction leaching of rare earth from ion-adsorption type rare earths ore with ferrous sulfate. *J. Rare Earths* **2016**, *34*, 917–923. [\[CrossRef\]](#)
9. Chen, Z.; Zhang, Z.Z.; He, Z.Y.; Chi, R.A. Mass transfer process of leaching weathered crust elution-deposited rare earth ore with magnesium salts. *Physicochem. Probl. Miner. Process.* **2018**, *54*, 1004–1013. [\[CrossRef\]](#)
10. Zou, H.L.; Zhang, Z.Y.; Chen, Z.; Liu, D.F.; Zhang, H.; Chi, R.A. Seepage process on weathered crust elution-deposited rare earth ores with ammonium carboxylate solution. *Physicochem. Probl. Miner. Process.* **2020**, *56*, 89–101. [\[CrossRef\]](#)
11. Luo, X.P.; Zhang, Y.B.; Zhou, H.P.; He, K.Z.; Zhang, B.Y.; Zhang, D.M.; Xiao, W.J. Pore structure characterization and seepage analysis of ionic rare earth orebodies based on computed tomography images. *Int. J. Min. Sci. Technol.* **2022**, *32*, 411–421. [\[CrossRef\]](#)
12. Wang, X.J.; Wang, H.; Sui, C.; Zhou, L.B.; Feng, X.; Huang, C.G.; Zhao, L.; Zhong, W.; Hu, K.J. Permeability and Adsorption–Desorption Behavior of Rare Earth in Laboratory Leaching Tests. *Minerals* **2020**, *10*, 889. [\[CrossRef\]](#)
13. Deng, Y.C.; Wan, Y.H.; Yu, H.D.; Kang, S.J.; Deng, Y.; Yang, J. Changes in Microfine Particle Migration of Ionic Rare Earth Ores during Leaching. *Sustainability* **2023**, *15*, 3867. [\[CrossRef\]](#)
14. Liu, D.F.; Zhang, Z.Y.; Chi, R.A. Microscopic Seepage Mechanism during In-situ Leaching of Weathered Crust Elution-deposited Rare Earth Ores. *Chin. Rare Earths* **2020**, *41*, 1–11. [\[CrossRef\]](#)
15. Wang, G.L.; Zhang, J.L.; Liu, Z.J.; Tan, Y.B.; Wang, Y.Z. Cracking and Microstructure Transition of Iron Ore Containing Goethite in Fe-C Melt Based on the Hismelt Process. *Minerals* **2023**, *13*, 448. [\[CrossRef\]](#)
16. Wang, Y.; Li, C.H.; Hou, Z.Q.; Yi, X.F.; Wei, X.M. In Vivo X-ray Computed Tomography Investigations of Crack Damage Evolution of Cemented Waste Rock Backfills (CWRB) under Uniaxial Deformation. *Minerals* **2018**, *8*, 539. [\[CrossRef\]](#)
17. Yin, S.H.; Chen, X.; Yan, R.F.; Wang, L.M. Pore Structure Characterization of Undisturbed Weathered Crust Elution-Deposited Rare Earth Ore Based on X-ray Micro-CT Scanning. *Minerals* **2021**, *11*, 236. [\[CrossRef\]](#)
18. Fan, N.; Wang, J.R.; Deng, C.B.; Fan, Y.P.; Wang, T.T.; Guo, X.Y. Quantitative characterization of coal microstructure and visualization seepage of macropores using CT-based 3D reconstruction. *J. Nat. Gas Sci. Eng.* **2020**, *81*, 103384. [\[CrossRef\]](#)
19. Li, Y.; Chi, Y.M.; Han, S.L.; Zhao, C.J.; Miao, Y.N. Pore-throat structure characterization of carbon fiber reinforced resin matrix composites: Employing Micro-CT and Avizo technique. *PLoS ONE* **2021**, *16*, e0257640. [\[CrossRef\]](#)
20. Keles, C.; Sarver, E. A Study of Respirable Silica in Underground Coal Mines: Particle Characteristics. *Minerals* **2022**, *12*, 1555. [\[CrossRef\]](#)
21. Liu, D.F.; Yan, W.X.; Zhang, Z.Y.; Chi, X.W.; Chi, R.A. Study on Fractal Leaching Kinetics of Weathered Crust Elution-deposited. *Rare Earth Chin. Rare Earths* **2021**, *42*, 1–9. [\[CrossRef\]](#)
22. Long, P.; Wang, G.S.; Tian, J.; Hu, S.L.; Luo, S.H. Simulation of one-dimensional column leaching of weathered crust elution-deposited rare earth ore. *Trans. Nonferrous Met. Soc. China* **2019**, *29*, 625–633. [\[CrossRef\]](#)
23. An, R.; Kong, L.W.; Zhang, X.W.; Li, C.S. Effects of dry-wet cycles on three-dimensional pore structure and permeability characteristics of granite residual soil using X-ray micro computed tomography. *J. Rock Mech. Geotech. Eng.* **2022**, *14*, 851–860. [\[CrossRef\]](#)

24. Zhang, X.; Gao, Z.; Rao, Y.; Shi, L.; Xu, W. Evolutionary Law of Pore Structure of Ion-Adsorbed Rare Earth Ore Leaching Process. *Minerals* **2023**, *13*, 322. [[CrossRef](#)]
25. Yan, B.H.; Wu, A.X.; Miao, X.X.; Liu, H.B. Microstructure evolution of ore particles during bioleaching based on X-ray Micro-Computed tomography images. *Adv. Mater. Res.* **2015**, *1130*, 325–328. [[CrossRef](#)]
26. Yan, B.H.; Wu, A.X.; Yin, S.H. Simulation of pore scale fluid flow of granular ore media in heap leaching based on realistic model. *J. Cent. South Univ.* **2011**, *18*, 848–853. [[CrossRef](#)]
27. Wu, A.X.; Yang, B.H.; Zhou, X. Fractal analysis of granular ore media based on computed tomography image processing. *Trans. Nonferrous Met. Soc. China* **2008**, *18*, 1523–2528. [[CrossRef](#)]
28. Chen, J.; Feng, Y.G.; Gu, R.G.; Shu, H.K.; Ba, L.Z.; Wei, L. Study on pore size effect of low permeability clay seepage. *Arab. J. Geosci.* **2019**, *12*, 238. [[CrossRef](#)]
29. Miao, X.X.; Li, S.C.; Chen, Z.Q.; Liu, W.Q. Experimental Study of Seepage Properties of Broken Sandstone Under Different Porosities. *Transp. Porous Media* **2011**, *86*, 805–814. [[CrossRef](#)]
30. Yan, B.H.; Wu, A.X.; Jiang, H.C.; Chen, X.S. Evolvement of permeability of ore granular media during heap leaching based on image analysis. *Trans. Nonferrous Met. Soc. China* **2008**, *18*, 426–431. [[CrossRef](#)]
31. Zhao, Y.X.; Zhu, G.P.; Liu, S.M.; Wang, L.; Zhang, C. Effects of Pore Structure on Stress-Dependent Fluid Flow in Synthetic Porous Rocks Using Microfocus X-ray Computed Tomography. *Transp. Porous Media* **2019**, *128*, 653–675. [[CrossRef](#)]
32. Li, G.Y.; Dai, S.; Zhang, L.T.; Chen, Y.M. A pore-scale numerical investigation of the effect of pore characteristics on flow properties in soils. *J. Zhejiang Univ. Sci. A* **2019**, *20*, 961–978. [[CrossRef](#)]
33. Chang, B.M.; Du, C.F.; Su, M.K.; Lin, Y.F.; Wang, Y.; Chu, X.F.; Zhang, L.; He, J.Q. Mesoscopic Seepage Simulation and Analysis of Unclassified Tailings Pores Based on 3D Reconstruction Technology. *ACS Omega* **2021**, *6*, 14309–14316. [[CrossRef](#)] [[PubMed](#)]
34. Zhou, G.; Zhang, Q.; Bai, R.N.; Ni, G.H. Characterization of Coal Micro-Pore Structure and Simulation on the Seepage Rules of Low-Pressure Water Based on CT Scanning Data. *Minerals* **2016**, *6*, 78. [[CrossRef](#)]

Disclaimer/Publisher's Note: The statements, opinions and data contained in all publications are solely those of the individual author(s) and contributor(s) and not of MDPI and/or the editor(s). MDPI and/or the editor(s) disclaim responsibility for any injury to people or property resulting from any ideas, methods, instructions or products referred to in the content.